Investigating the effect of metal powder recycling in Electron beam Powder Bed Fusion using process log data

Sujana Chandrasekar[1], Jamie B. Coble[1,2], Sean Yoder[3], Peeyush Nandwana[3], Ryan R. Dehoff[3,4], Vincent C. Paquit[3], Sudarsanam S. Babu[1,3,4]

[1]The Bredesen Center for Interdisciplinary Research and Graduate Education, [2]Department of Nuclear Engineering, The University of Tennessee, Knoxville TN 37996; [3]Manufacturing Demonstration Facility, Oak Ridge National Laboratory, Oak Ridge, TN 37831; [4]Department of Mechanical, Aerospace and Biomedical Engineering, The University of Tennessee, Knoxville, TN 37996

Declaration of interests: None

Research sponsored by the U.S. Department of Energy, Office of Energy Efficiency and Renewable Energy, Industrial Technologies Program, under contract DE-AC05-00OR22725 with UT-Battelle, LLC.

Contents

Abstract

Recycling metal powders in the Additive Manufacturing (AM) process is an important consideration in affordability with reference to traditional manufacturing. Metal powder recyclability has been studied before with respect to change in chemical composition of powders, effect on mechanical properties of produced parts, effect on flowability of powders and powder morphology of parts. However, these studies involve *ex situ* characterization of powders after many use cycles. In this paper, we propose a data-driven method to understand *in situ* behavior of recycled powder on the build platform. Our method is based on comprehensive analysis of log file data from various sensors used in the process of printing metal parts in the Arcam Electron Beam Melting (EBM) ® system. Using rake position data and rake sensor pulse data collected during Arcam builds, we found that Inconel 718 powders exhibit additional powder spreading operations with increased reuse cycles compared to Ti-6Al-4V powders. We substantiate differences found in *in situ* behavior of Ti-6Al-4V and Inconel 718 powders using known sintering behavior of the two powders. The novelty of this work lies in the new approach to understanding powder behavior especially spreadability using *in situ* log file data that is regularly collected in Arcam EBM® builds rather than physical testing of parts and powders post build. In addition to studying powder recyclability, the proposed methodology has potential to be extended generically to monitor powder behavior in AM processes.

Keywords

Electron beam Powder Bed Fusion (E-PBF); Ti-6Al-4V; Inconel 718; Data-driven analysis; Powder recycling

1. Introduction

Additive Manufacturing (AM) has evolved to become a viable option for industrial production of parts with complex geometry, especially in the aerospace, medical and nuclear industries [1–3]. This is primarily because of reduced waste generated in the AM process, the ability to manufacture parts that have intricate and complex geometric features for specific functions, and aerospace parts that have high buy-to-fly ratio compared to traditional manufacturing [2]. These enablers are especially desirable for parts made of expensive metals like titanium where waste reduction leads directly to cost savings. In this context, the affordability of material feedstock used in AM can be further improved with recycling of metal powders used in the process. However, given the critical function performed by the AM parts, particularly in safety-critical applications like aerospace and nuclear power, it is important to ensure quality of parts made by recycled powders is equivalent to that of fresh powders.

Many studies have been performed to understand powder recyclability with regard to its effect on particle morphology [4], flowability [4–6], particle size distribution [2,4,7], and oxygen pickup [2,4,6–8]. A brief review of powder recyclability studies in the Electron beam- Powder Bed Fusion (E-PBF) process and Selective Laser Melting (SLM) process literature is given here. Common trends emerge since both processes are powder bed fusion processes. Recycling of Ti-6Al-4V powders led to an increase in oxygen content [2,4,6–8], which was the limiting factor in powder reuse for various applications [2,8]. The effect of increased oxygen content on mechanical properties of titanium parts has been studied by various groups with the conclusion that oxygen increased part strength but lowered ductility and toughness [9–12]. These conclusions were shown to hold for parts made of recycled titanium powder [7] due to the increase in oxygen content in powder. Contradictory conclusions were reached by research groups [4,5]

on effect of recycling on flowability of powder. A study on the effect of recycling on fatigue life [13] indicates that recycled Ti-6Al-4V powder led to parts with lower elongation and reduced breakage area even after Hot Isostatic Pressing that typically closes pores and improves properties. In summary, effects of recycling Ti-6Al-4V powder on part and powder properties have been studied using *ex situ* analysis methods by different research groups.

There is limited literature on recycling of Inconel718 powder. In general, research papers [8,14,15] report an increase in powder agglomeration and particles becoming less spherical in shape with increased recycling of Inconel718 powder.

Recyclability studies cited above have varied in their approach but a general framework was proposed by Cordova et al. [16]. The framework consisted of tests to decide whether a powder can be reused in the SLM process based on measured properties like particle shape, powder flowability, chemical composition, and density. It can potentially be extended to the E-PBF process too. Standards developed for characterization of metal powders for AM and their systematic use has been provided by Slotwinski et al. [17]

The above mentioned studies around recyclability have focused on *ex situ* characterization to understand the effect of recycling Ti-6Al-4V and Inconel718 powders in the E-PBF or SLM processes. *Ex situ* characterization can be time consuming and expensive. We propose *in situ* characterization of powder behavior using data stored in log files, i.e. data from in-built sensors in the Arcam Electron Beam Melting (EBM)® system. Information about Arcam EBM ® software and log files can be found in chapter 5 of [18]. To our knowledge, only one other published work i.e. Grasso et al. [19] has focused on using log file data to understand build characteristics. While Grasso et al. focused on distinguishing between in-control and out of control builds, our work is focused on understanding powder behavior using log file

data.In this paper, we demonstrate a data analysis method to study powder behavior, especially spreadability, in the E-PBF process. Our hypothesis is that data collected in the log file of the Arcam EBM® system can be used to understand rake motion and thereby powder spreading during the build process. We expect powder behavior on the build table to change due to reuse of powder and want to explore whether the change can be detected using log file data. We therefore use data collected during powder recyclability tests of Inconel 718 and Ti-6Al-4V alloy powders that has been published earlier [8].

The paper is organized as follows: Section 2 contains a brief description of E-PBF builds used in this study. Section 3 presents an overview of the relevant mechanics of the Arcam machine and outlines the data available in log files used in this study. Section 4 describes the data analysis approach in detail. Section 5 contains results of this data analysis method on recycled powder build log files. Conclusions drawn from this study and potential areas of future work are summarized in Section 6.

2. Experimental details

Experimental data in this paper is based on log files, generated by the Arcam EBM® system, of builds used to study powder recyclability by Nandwana et al. [8]. The Arcam EBM® system is an E-PBF system to build metallic parts layer-by-layer. In their work, Nandwana et al. studied recyclability of Inconel 718 and Ti-6Al-4V alloy powders in the EBM® process using an Arcam A2 machine. They built six builds using Inconel 718 and five builds using Ti-6Al-4V powder. The build geometry is shown in Figure 1. The first two Ti-6Al-4V builds reached >88% of planned build height but failed to complete due to arc trip issues. They are therefore excluded from recyclability analysis but presented for completeness by Nandwana et al. [8]. We consider log file data from all five builds of Ti-6Al-4V in our analysis to aid

comparison with results presented by Nandwana et al. [8]. Similarly, the fifth build of Inconel 718 failed to complete but is included for completeness in comparison with Nandwana et al. [8].

The recycling process is depicted schematically in Figure 2 and described here. The build process started with approximately 100 kg of the alloy powder. The first build was intended to be the tallest and its height was designed to target complete emptying of powder hoppers at the end of the build. This was done to ensure that all powder would be exposed to electron beam before being recycled. Build heights did not line up in descending order due to powder spillage and failed builds, as described in the results section of this paper. Once completed, the build was removed from the Arcam build chamber (dotted red arrows in Figure 2) and leftover powder in the chamber was vacuumed (dashed blue arrows in Figure 2) and collected. A small quantity of powder fell through the powder sensors as required by the Arcam EBM ® rake control system. This will be explained in the following section of the paper. Powder in powder sensors was discarded from the study. Partially sintered powder from the external surface of the build was recovered using the Powder Recovery System (PRS) in the Arcam EBM® system. The vacuumed powder was mixed with recovered powder from PRS and sieved on a vibratory sieve through a 100-mesh (150 microns). Powder particles remaining in the sieve, i.e. particles bigger than 150 micron, were discarded. A sample was collected from the sieved powder for *ex situ* analysis. The sieved, recycled powder (dot-dash green arrow in Figure 2) was then emptied into the two powder hoppers and the next build was printed. This process was repeated till the target number of builds had been built. As a part of the qualification and validation of AM processes, the underlying log files were stored, but never analyzed. This research focuses on using these data to understand powder behavior, specifically powder spreadabuility, during the build process.

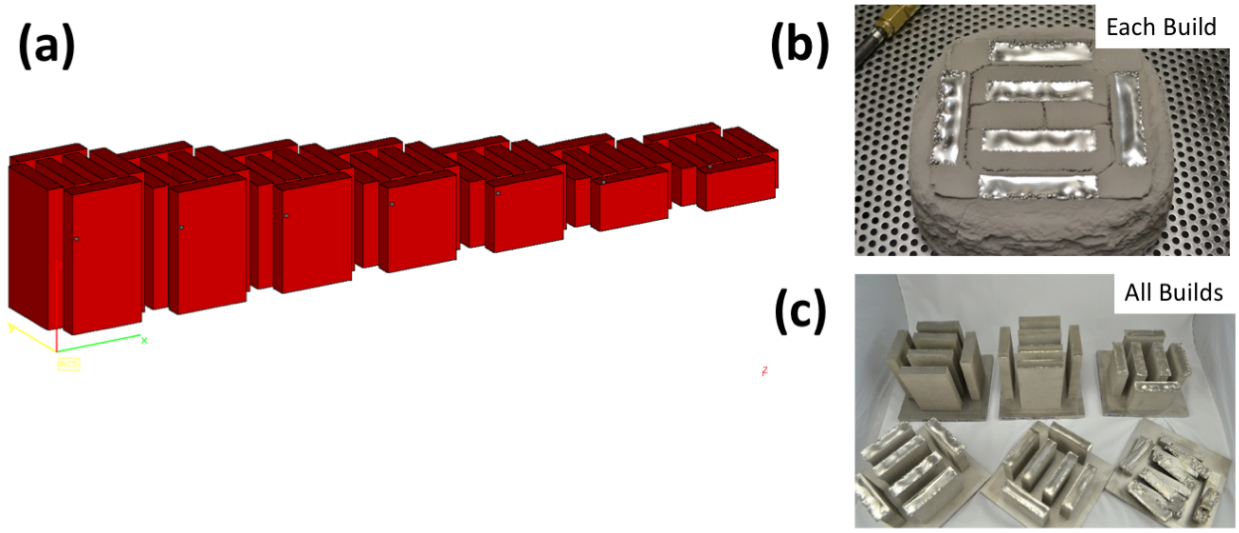

Figure 1: (a) Schematic of build design used in recyclability study [8]. After each build, the height of the next build was reduced to allow for the reduction in the total available powder; (b) Partially sintered powder can be seen on the exterior surface of the build before the powder recovery operation. (c) Final finished builds are shown with 1 failed build

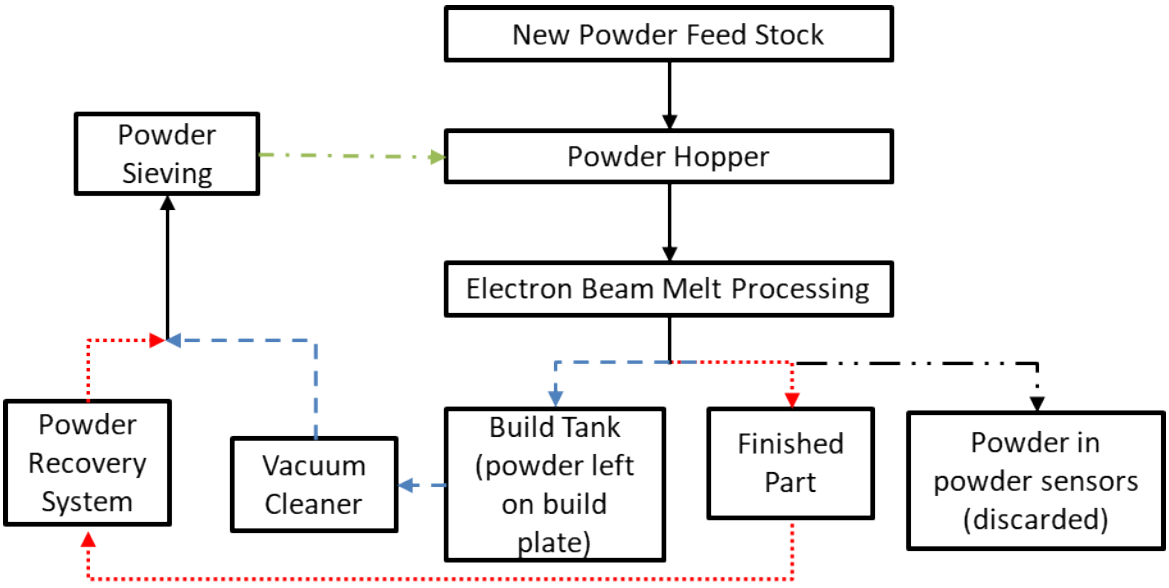

Figure 2: Schematic of powder recycling process used in recyclability study. Adapted from [8].

3. Operation of Arcam EBM ® and rake control logic

A brief description of the working of the Arcam EBM® system is presented here. The Arcam EBM ® system is shown schematically in Figure 3, Figure 4 and Figure 7. The system consists of a vacuum chamber which contains an electron beam generation and deflection system, two powder hoppers, a build platform, a rake and two powder sensor collection bins beneath the build table. The powder hoppers are gravity driven and deposit powder as mounds at the two ends of the build platform. The rake starts the build process by spreading a preset thickness of powder across the build platform. Some powder on the build plate falls through the powder sensor at either end and is used as a control signal for rake movement as described later in this section. A de-focused electron beam pre-heats powder that has been spread on the build table at the start of the build. The aim of pre-heating is to partially sinter powder so that these powders melt without issues like "smoking" [20] during the build process. After the pre-heat step, a focused electron beam traces a path along the powder bed that corresponds to the cross-section to be built. Powder along the beam path melts and forms a layer of the part being built. Once a layer is completed, the build platform is lowered by a preset height and the steps above are repeated to build the next layer.

For each of the builds described in Section 2, log file data were generated by Arcam EBM® and stored. Arcam log files record process parameters over the course of the build. The parameters used in this paper are rake position, rake sensor pulse and layer height, all recorded with corresponding time stamps. Rake position is the horizontal position of the rake along the build platform. Rake position changes as a function of time when powder is being spread on the build platform. Rake sensor pulse signal measures the time for which powder falls through the powder sensor as the rake spreads powder. It is an indirect

measure of quantity of powder that falls through the powder sensors. Layer height records the height of the build after each layer is completed.

The data associated with analysis in this paper has been archived and is available at the link provided in the appendix.

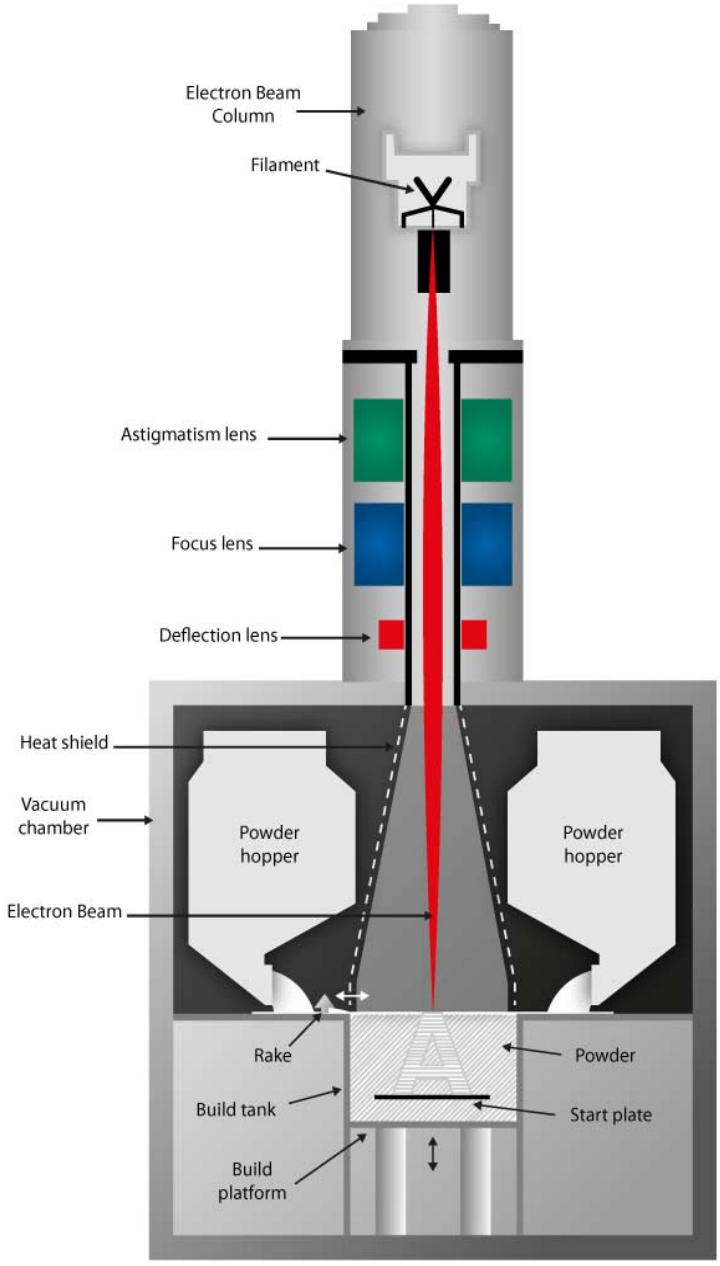

Figure 3: Arcam EBM® system schematic (Source: http://www.arcam.com/technology/electron-beam-melting/hardware/)

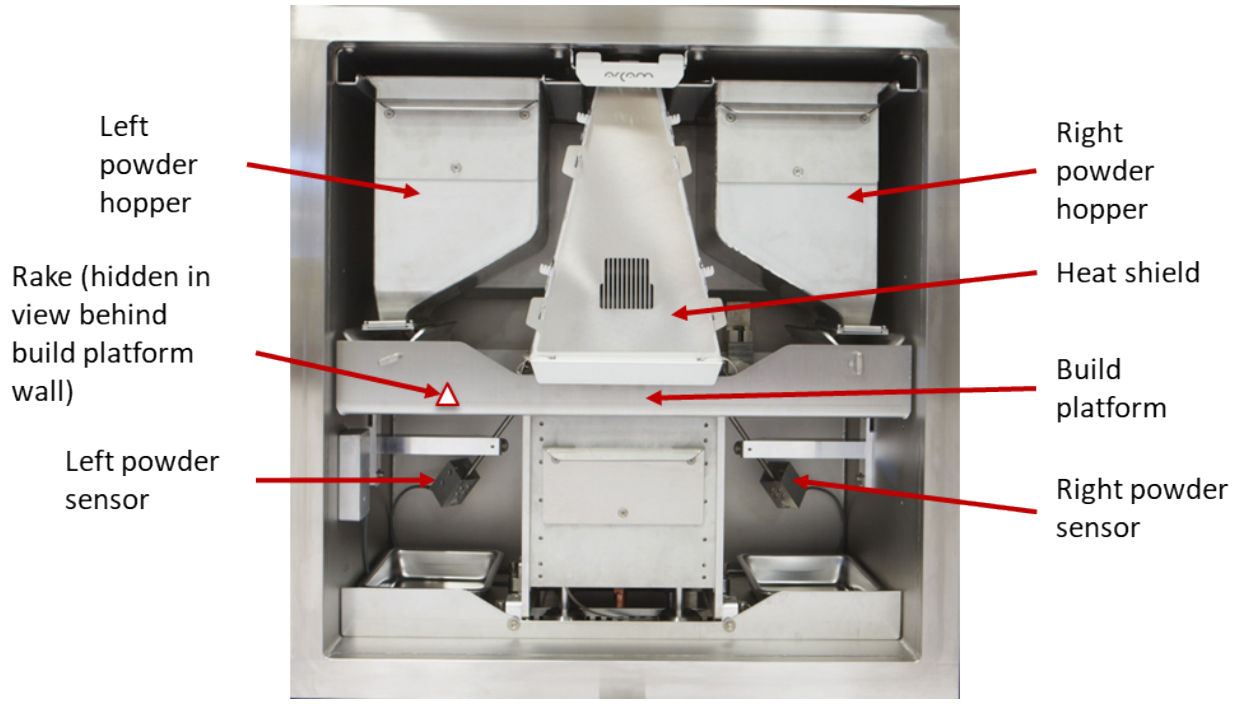

Figure 4: Inside view of Arcam EBM ® system. Powder hoppers, powder sensors, build platform and heat shield are seen.. Adapted from: http://www.arcam.com/technology/electron-beam-melting/hardware/

The analysis in this research focuses on rake motion as an *in situ* indicator of powder characteristics, specifically powder spreadability. For ease of reference, we define terms associated with data analysis. A "layer print" is the period over which the electron beam is turned on and a layer is being printed. "Rake event" refers to the motion of the rake across the build platform. This occurs between successive layer prints. Figure 5 shows two rake events and a layer print in between. During a layer print, the rake position remains constant as the rake is stationary at one end of the build platform. A "rake pass" refers to motion of the rake from one end of the build platform to the other. The set of rake passes that occur between two layer prints comprise the rake event.

Our analysis is based on data collected during rake events i.e. when the rake is in motion and interacting with the powder. Rake motion may proceed under default or abnormal conditions depending on rake sensor pulse values. Under normal conditions, the rake event consists of three rake passes, shown in Figure 5. In the first pass, the "fetch powder" pass, the rake moves into the powder mound closest to it, fetches powder and spreads it across the build platform. The next two passes are "spread powder" passes where the rake does not fetch additional powder but only spreads existing powder across the build platform. In an abnormal condition, also shown in Figure 5, the rake carries out additional fetch powder passes till a stopping criterion is met and then spreads powder in two spread powder passes. The additional fetch powder passes are referred to as "re-raking" passes.

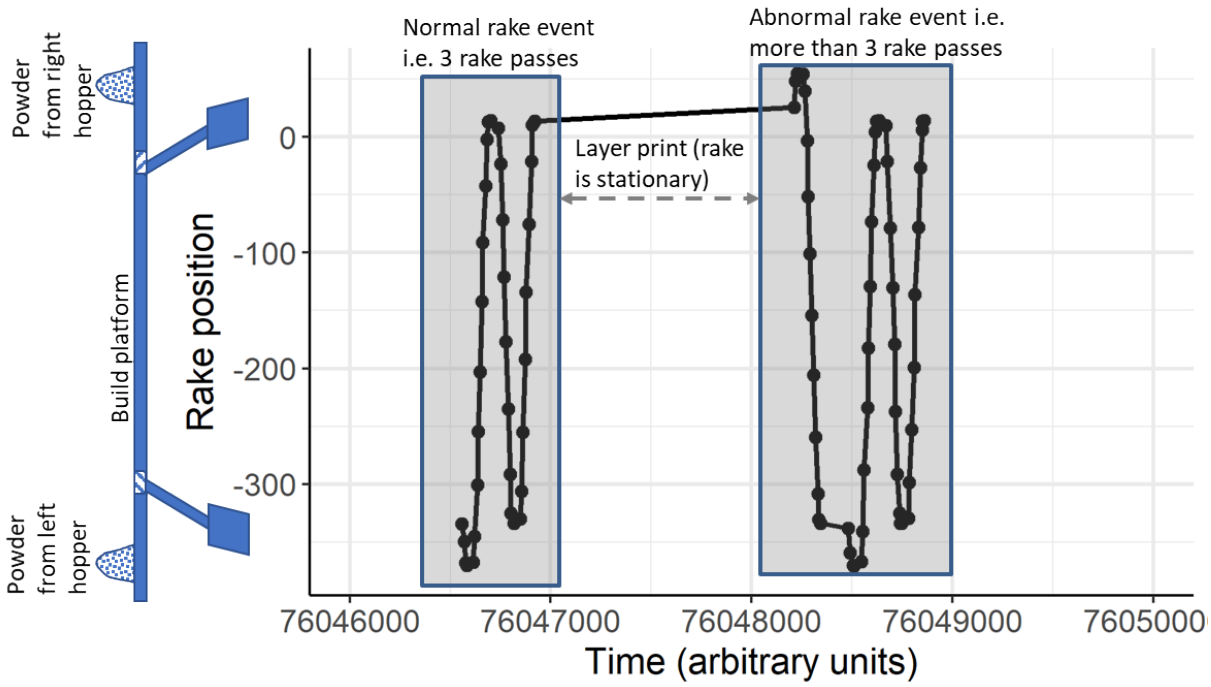

Figure 5: Two rake events are shown alongside position on the build platform. A normal rake event has three rake passes whereas an abnormal rake event has more than three rake passes.

The decision to re-rake or not is based on rake sensor pulse values measured during the fetch powder pass [21]. This is described in Figure 6. Each rake sensor pulse is only labeled as left or right sensor pulse in the log file. To understand rake control logic, we re-label this as near end or far end pulse depending on rake position at the start of the rake event. As the names indicate, near end pulse refers to pulse of rake sensor nearer to the rake starting position while far end pulse is the pulse of rake sensor farther from the rake starting position. Each rake sensor has a minimum and maximum acceptable pulse value associated with it. It also has a maximum allowable count of invalid pulses. If the far end rake sensor pulse during the fetch powder pass is outside acceptable rake pulse values, an invalid pulse is generated. Additional fetch powder passes are carried out till one of two conditions is met : The far rake sensor pulse value is

within prescribed limits OR number of far end invalid pulses exceeds set threshold. When this happens, the system determines that the far end sensor is temporarily broken and proceeds with two spread powder passes to complete the rake event. Interestingly, the invalid pulse count is carried over between layers and reset only when a valid pulse is encountered. Upon checking log files, it was found that re-raking control logic described in Arcam EBM ® manual did not hold for 4 out of more than 20000 layers that were analyzed. These layers do not change results of the study in any way since we analyze gross re-raking trends and not layer-specific ones (see results section).

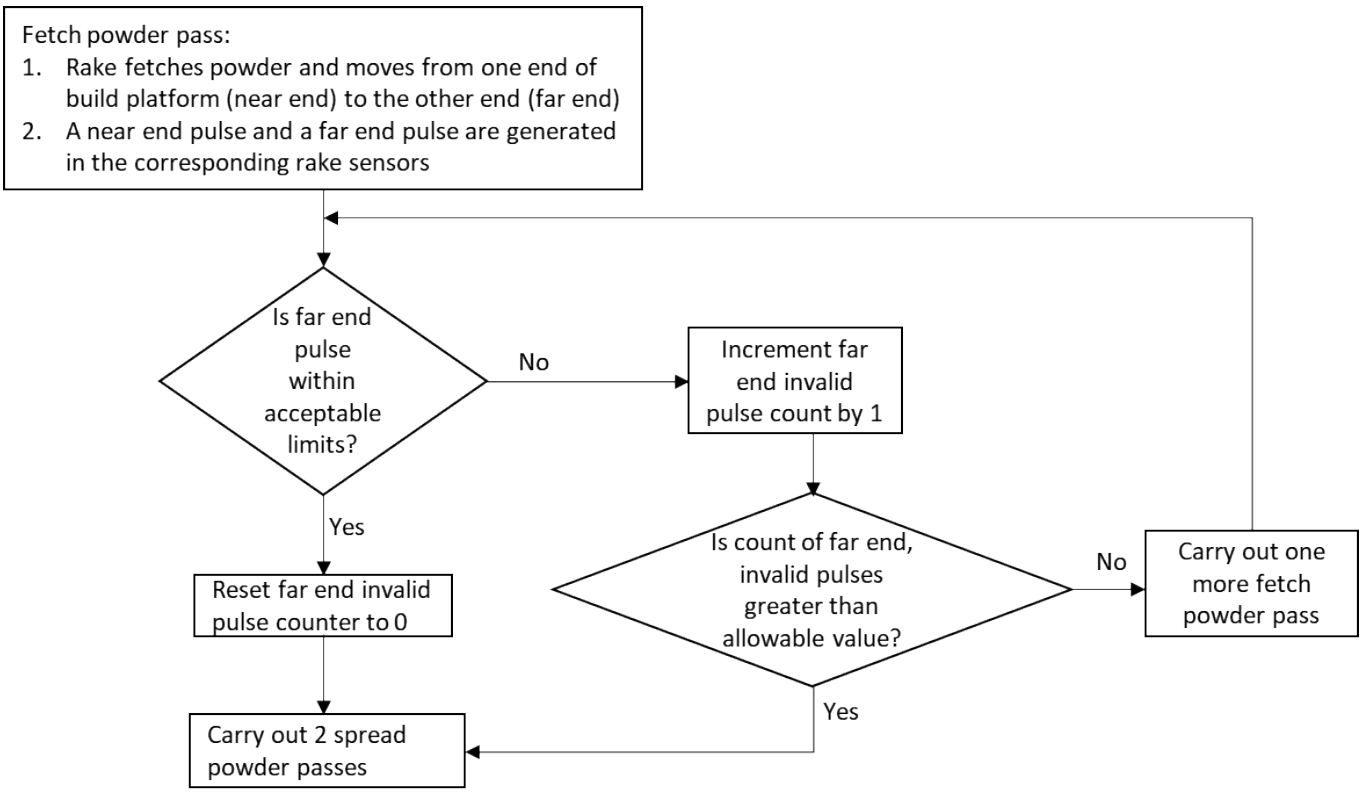

Figure 6: Rake control regulation logic based on rake pulse values

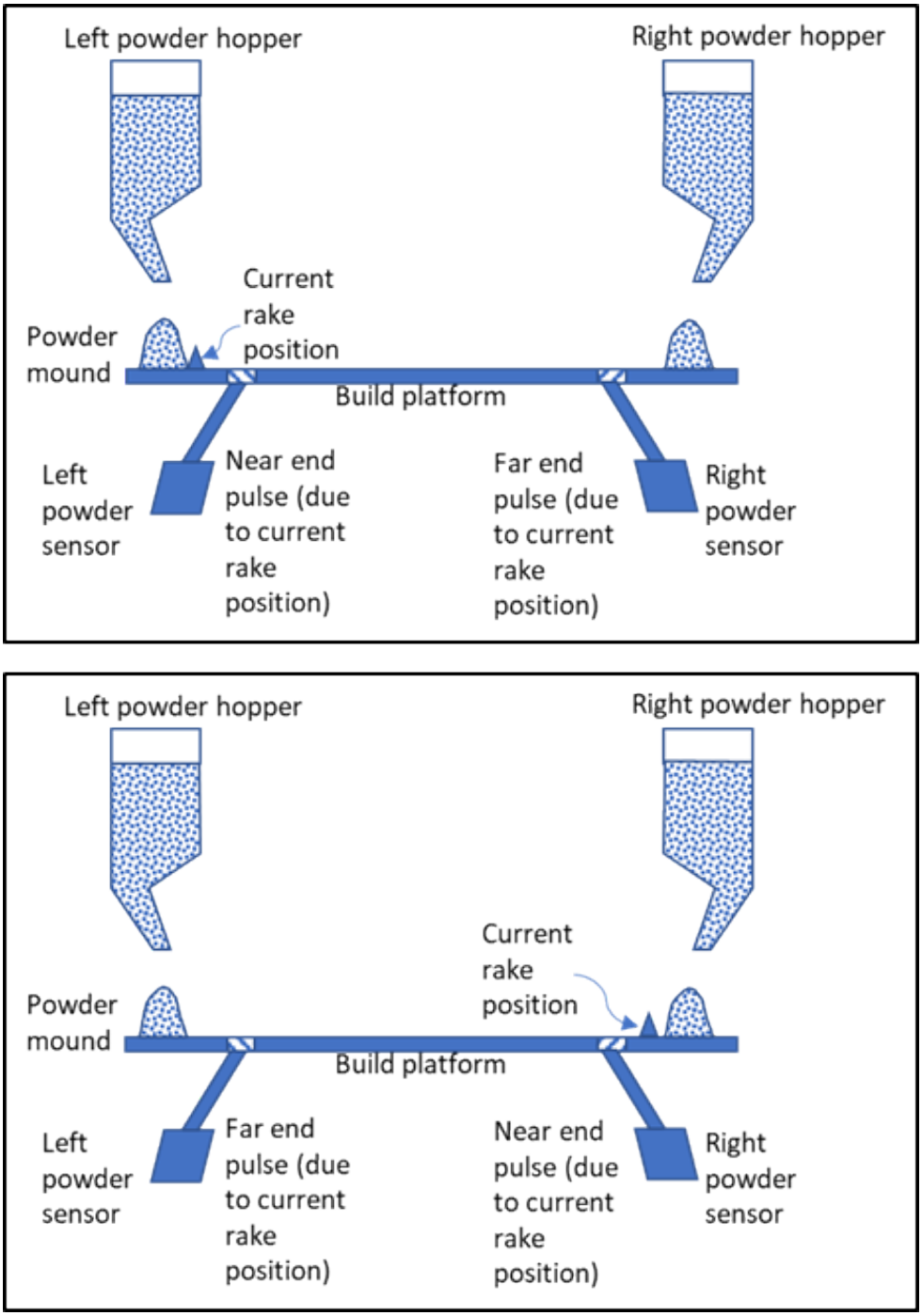

Figure 7: Schematic showing rake near end and far end corresponding to the current rake position

4. Data analysis approach

This section describes the data analysis approach used in this paper. A flowchart that depicts data analysis of rake position and rake sensor pulses is given in Figure 8. The details of each step of the flowchart are explained in the following subsections.

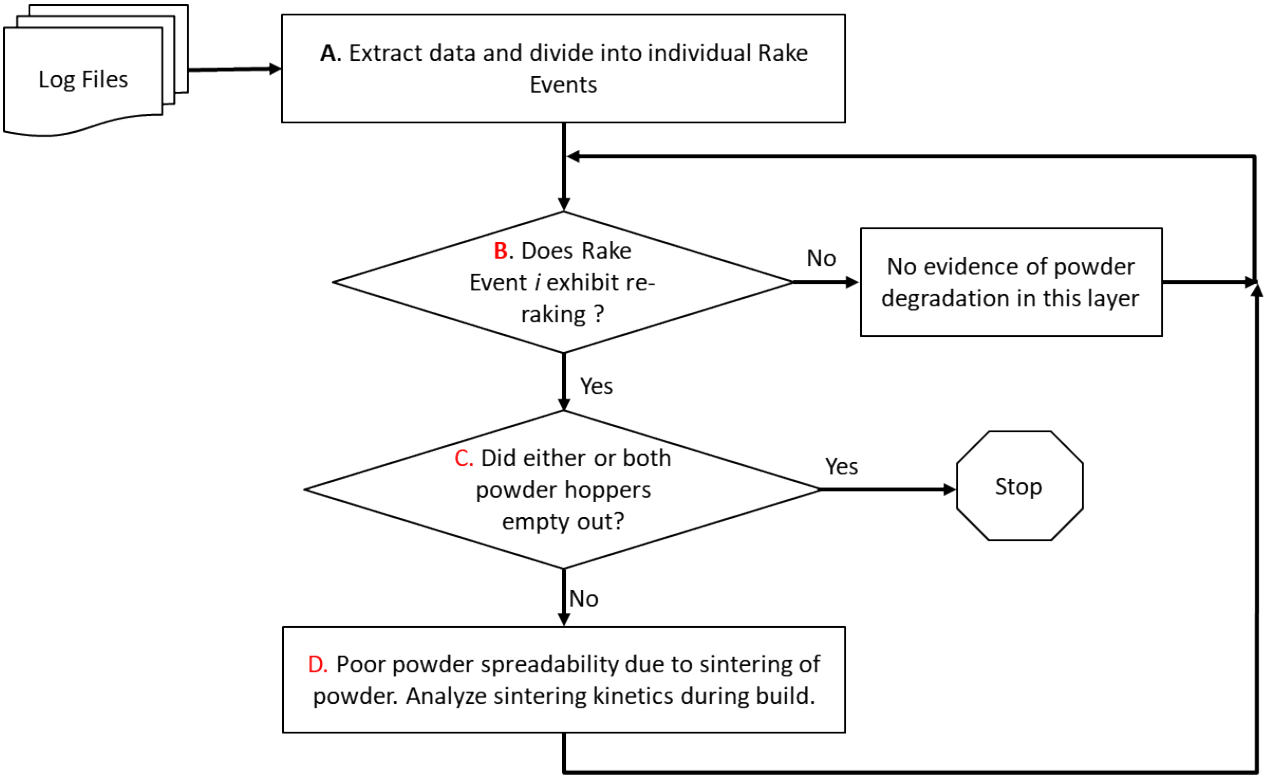

Figure 8: Flowchart showing data analysis steps in analyzing log files from Arcam EBM® system

Step A:

Step A extracts rake position data from the build log files. The rake position data are divided into separate rake events by indexing rake position off the time stamp associated with build platform height. Build

platform height is a variable in the log file that gets updated when the build platform is lowered at the end of each layer print. Its time stamp can be used as an indicator commencement of a rake event based on which rake position data can be indexed by layer. After the log file data are divided into individual rake events, each rake event *i* is evaluated in turn to determine if each layer (a) exhibits evidence of powder problems, or (b) indicates that one or both hoppers have emptied and insufficient powder is available, in which case analysis is halted. These steps are explained in detail below.

Step B:

Step B analyzes rake position data for a specific layer to compute the total number of rake passes and determine if re-raking has occurred. The number of rake passes per rake event can be computed by counting rake position data points, which are collected at fairly regular intervals of time during rake motion, and thus the number of rake position data points per fetch powder pass or spread powder pass is roughly constant. The number of rake passes, N_r, can be calculated according to equation (1) after determining the average number of data points per spread powder pass, N_s, and fetch powder pass, N_f, manually from the first few layers.

$$N_r = \left\| \frac{N - 2N_s}{N_f} \right\| + 2 \tag{1}$$

where N is number of data points in rake event and $\| . \|$ indicates rounding to nearest integer. This method of calculating the number of rake passes has been verified by plotting rake position over time from the log file for ten randomly selected rake events per build to ensure that the method calculates the correct number of rake passes per rake event. Across theavailable builds, Inconel 718 builds and Ti-6Al-4V

builds have different frequency of data collection of rake position and therefore have different numbers of data points, N_s and N_f, per spread powder and fetch powder pass, respectively; however, the consistency of data collection within builds of each material type remains.

Figure 9 shows the number of data points for each rake event (i.e. at the end of each build layer) in the first build of Ti-6Al-4V as indicated in the primary y-axis (on the left) while the secondary y-axis (on the right) indicates the number of rake passes per rake event. The color and shape also indicate the number of rake passes. A "normal" rake event would have 3 rake passes. Figure 9 shows that, in this build, mostly normal raking (3 passes) or 1 additional pass (4 passes in all) occurred prior to layer 1500. After layer 1500, the number of layers with 1 additional pass increased significantly. After layer 2500, the number of rake passes began to increase beyond 4 until all additional raking stopped at layer 2729. The cause of this behavior is explored in step C.

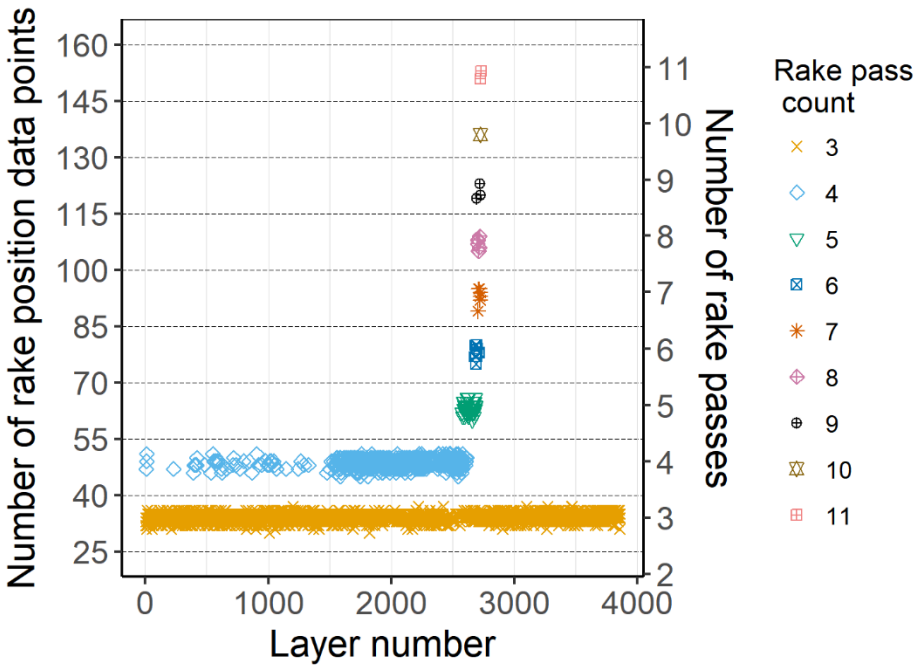

Figure 9: Rake position data point count plotted against layer number for Ti-6Al-4V Build 1 shows a rapid increase in re-rake events at around layer number 2500

If rake position data are collected at irregular intervals of time, this method of computing number of rake passes would not be appropriate. In that case, the number of rake passes could be determined by calculating the total distance traveled by the rake in each rake event:

$$d = \Sigma_i |r_i - r_{i-1}| \tag{2}$$

where r_i is the rake position at the i^{th} data point. The distance traveled would be proportional to number of fetch and spread powder passes per rake event.

If analysis of rake position indicates there are no additional rake passes beyond 3, then there is no evidence of powder problems in the current layer *i* and the analysis moves to the next layer *i+1*. If additional passes occured, potential causes are investigated in steps C and D.

Step C:

In step C, analysis of rake position and rake sensor pulse data determines if additional rake passes are a result of one or both hoppers emptying. Hopper emptying can be identified by evaluating the extreme rake position for the fetch powder pass of each rake event. Figure 10 shows plots of the extreme rake position during fetch powder passes of rake events for a given build. The corresponding positions on the build platform are shown schematically on the left. In other words, Figure 10 shows the position inside the powder mound where the rake moved to fetch powder. The plot on the left shows the left and right fetch powder positions while the two sides are zoomed in on the right. In the initial layers of the build, the rake does not go deep into the powder mound to fetch powder. As the part is printed, the rake moves further into the powder mound to fetch powder because the rake finds insufficient powder close to its resting position. The Arcam EBM® system uses rake sensor pulse as a control signal to compute the depth inside the powder mound to which the rake must move to "fetch" powder [21]. A characteristic sign of powder hopper emptying is that the rake moves to the maximum allowable position on the build platform to fetch powder. This is referred to as "rake position max out" and has been observed consistently across a variety of builds when either hopper empties. When the rake finds that no more powder is available, it moves to the other end of the platform to fetch powder. When both hoppers empty, the rake re-rakes repeatedly until the maximum allowable invalid pulse count is reached (as seen at layer 2729 in Figure 9). At this point, the rake sensor is deemed temporarily broken by the system and the layer is completed with 2 spread powder passes. It is important to note that even after hoppers empty out as

indicated by extreme end positions of the rake, the Arcam EBM ® system continues building the part. This may be because the system accounts for the possibility of a broken rake sensor. When part build occurs beyond hopper emptying, the part may be prone to defects due to insufficient powder availability during final build layers. Figure 10 illustrates extreme rake positions across layers of the build for which rake passes are shown in Figure 9. Figure 10 exhibits insufficient powder due to hopper emptying. As inferred from Figure 10, the right hopper empties out approximately at layer 1500 while the left hopper empties out approximately at layer 2500.

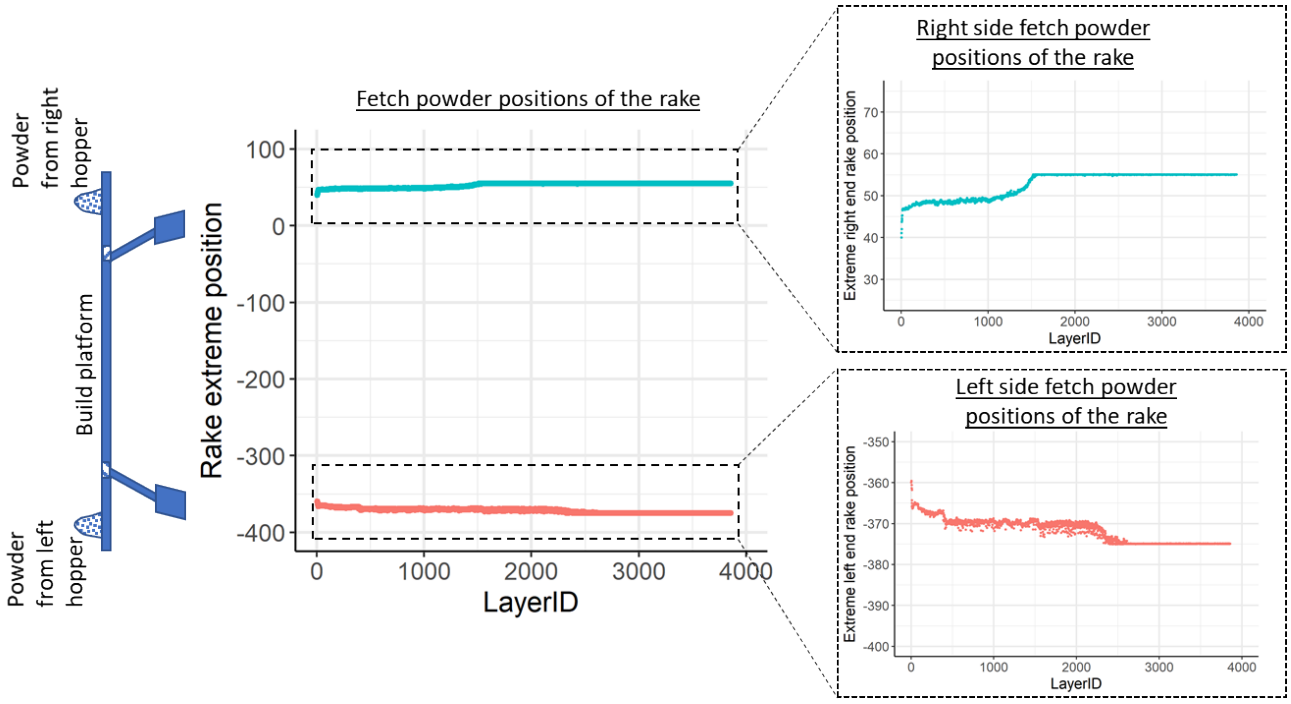

Figure 10: Rake extreme positions shown for each fetch powder pass in each rake event for the first build of Ti-6Al-4V

Rake position analysis described above indicates if either (or both) hopper(s) emptied. If log files indicate that rake hoppers did not empty out during the build, then additional rake passes detected in Step B were caused by other reasons of low rake sensor pulse. This is investigated in Step D.

Step D:

If hoppers did not empty but additional rake passes occurred, we hypothesize that particle sintering occurred on the build platform, leading to low rake sensor pulse. Particle sintering can lead to powder agglomeration, resulting in poor powder spreadability on the build platform and therefore insufficient powder flowing through the rake sensor. There is no existing metric to evaluate *in situ* powder spreadability [22] but we can use basic sintering kinetics to analyze if our hypothesis points in the direction of powder agglomeration. We can also use *ex situ* SEM images of powder samples to check for powder agglomeration. A note of caution with SEM images is that *ex situ* powder analysis is done on powder after it is put through the PRS system and the sieve. So, signs of particle sintering and agglomeration may not be seen clearly. Ultimately, the effects of poor powder spreadability on part quality must be understood. Particle sintering and part quality analysis are beyond the scope of the current research and are potential areas of future work.

5. Results

Results from data analysis described in the previous section are presented for all builds described in Section 2 and included in previous work by Nandwana et al [8].

We start with Inconel 718 builds, which had five successful builds (build 5 failed at less than 35% of intended build height). Figure 11 shows the rake position-based analysis results for the number of rake passes in Inconel 718 builds. Build 1 was made with virgin powder while Build 6 has powder that has been recycled four times (Build 5 failed, and powder was not exposed to the electron beam from that build). Build 1 did not have pulse data recorded in the log file due to lack of positional orientation between powder sensors and build platform, resulting in default rake passes. Results presented in this section do not change when we exclude build 1 from the discussion; we have included it for ease of comparison with Nandwana et al. [8]. Following the steps in the data analysis flowchart (Figure 8), there is evidence of hopper emptying in all Inconel718 builds except build 5. Ignoring layers built after either hopper started emptying, we are left with fewer layers to analyze powder behavior change due to recycling. Table 1 summarizes the percentage of layers that had additional rake passes due to powder-related issues and not due to hopper-emptying issues for Inconel 718 builds. From Table 1, we observe that increased powder recycling led to increased rake passes after build 3, and this increase cannot be attributed to hopper emptying. We use sintering kinetics to explain powder agglomeration that may have happened and support our hypothesis using SEM images. Sintering kinetics are presented later in this section. SEM images published by Nandwana et al. [8] (reproduced in Figure 12) indicate powder particle agglomeration in Inconel718 powder with multiple reuse cycles. Since SEM images were taken after recycling powder through the PRS and sieve, they are not completely representative of changes in powder on the build plate but indicate broad trends. From the PSD (Figure 12), we observe an increase in large-sized particles with increased powder recycling and an accompanying increase in average powder particle diameter. The PSD indicates that virgin powder had many large particles but, after Build 1, the PSD changed significantly, hinting that large particles present in virgin powder may have been sieved out. Our

finding of powder agglomeration in recycled powder is in agreement with findings of other research groups [8,14,15,23,24] who studied Inconel 718 powder recycling in the SLM and E-PBF processes.

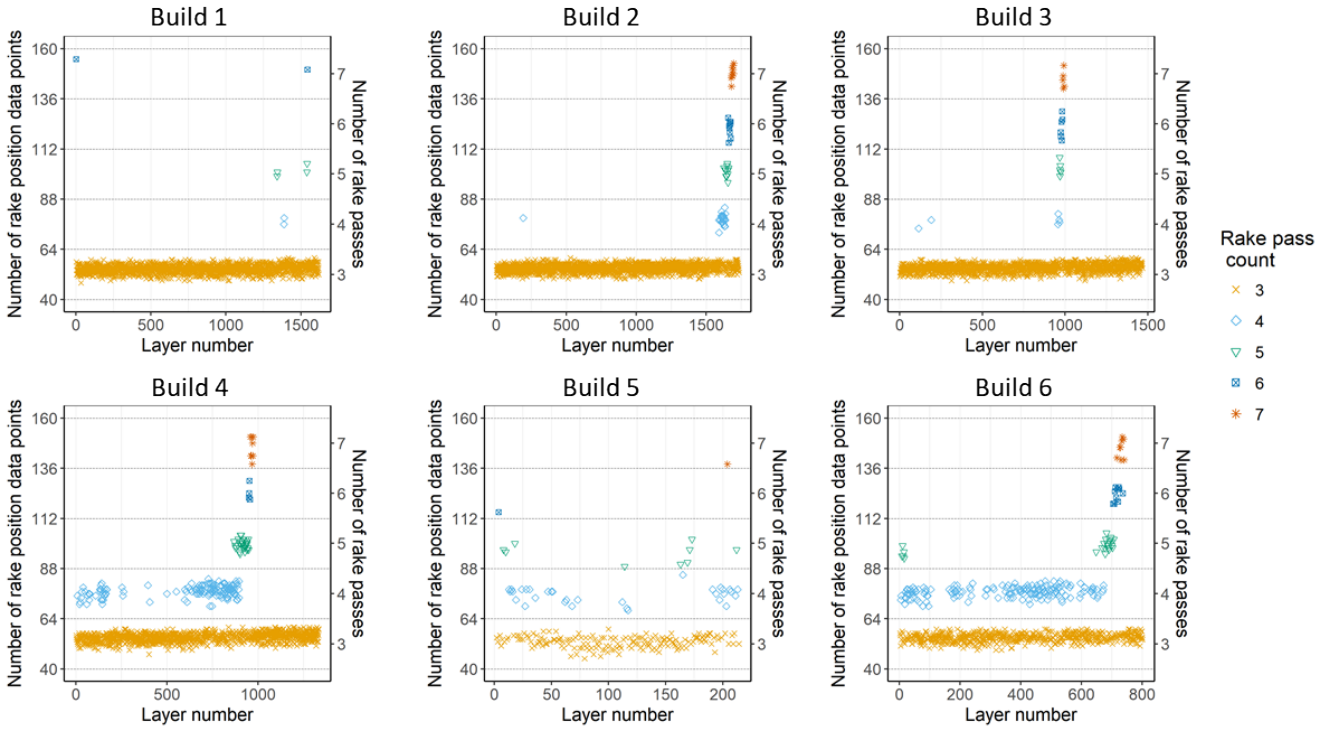

Figure 11: Data analysis results for Inconel 718 builds

Table 1: Re-raking in Inconel 718 before hoppers empty out

Build serial number	Number of layers printed	Layer number at which first hopper showed evidence of emptying	Number of re-raked layers prior to hopper emptying	Percentage of layers before hopper emptying with re-raking
1 (excluded from analysis due to improper alignment of powder sensor)	1618	1300	1	0.1 %
2	1733	1500	1	0.1%
3	1467	900	2	0.2%
4	1333	700	62	8.9 %
5 (excluded from analysis since it failed early)	214	*No clear trend seen due to erratic build*	-	-
6	800	550	143	26 %

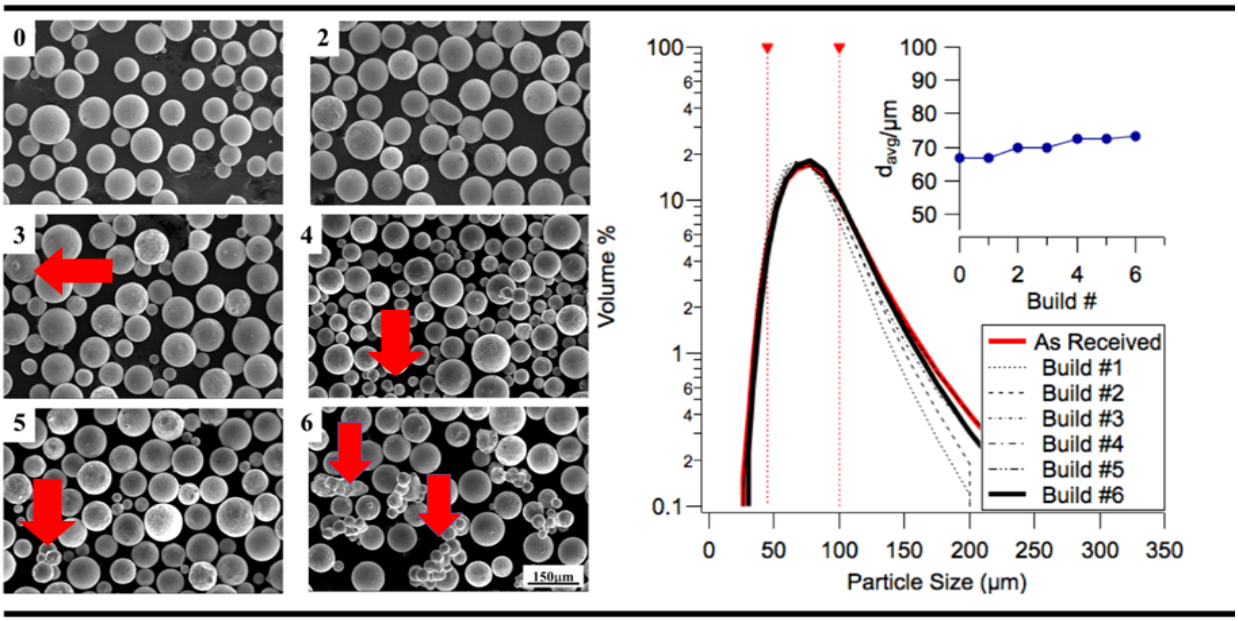

Figure 12: (left) SEM images showing particle shape of Inconel 718 powder after each reuse cycle and (right) particle size distribution of Inconel 718 powder after each powder reuse cycle (reproduced from [8] with permission)

The results of analysis of the five Ti-6Al-4V builds are shown in Figure 13. It is to be noted that builds 1 and 2 were failed builds as mentioned by Nandwana et al. [8] and are included only for comparison and completeness. They do not affect our conclusions in any way.

Only builds 1 and 4 indicate emptying of both powder hoppers. The percentage of layers experiencing re-raking not attributable to hopper emptying, summarized in Table 2, remains roughly constant across Ti-6Al-4V builds after the first build. This is in contrast to the results seen in Inconel 718 builds. We examine sintering kinetics of Ti-6Al-4V later in this section to reason out this behavior. SEM images of powder samples and resulting Powder Size Distributions (PSDs) are shown in Figure 14 (reproduced

from Nandwana et al. [8]). The PSDs were analyzed using a Horiba LA-950 Laser Diffraction Particle Analyzer [8]. The SEM images look similar across reuse cycles and all of them indicate the presence of a few satellite particles as shown by red arrows on most large powder particles. The PSD also indicates that powder sampled after Builds 2, 3, and 5 all have very similar size distributions. The PSD in Figure 14 suggests that Ti-6Al-4V powder does not exhibit an appreciable and persistent change in particle size that persists across powder with increased reuse cycles. This finding is in agreement with results in [16]where Ti-6Al-4V powder size distribution showed little variation after eleven cycles of reuse in a SLM process.

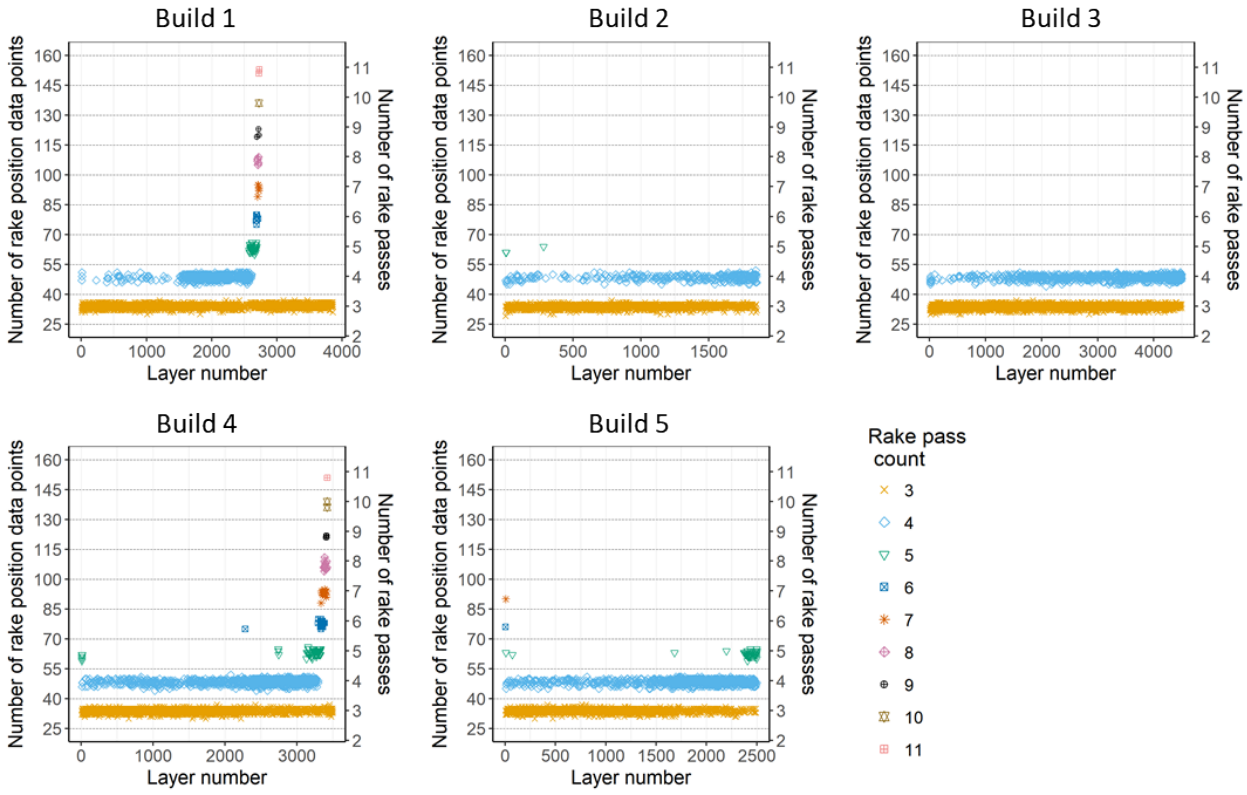

Figure 13: Data analysis results for Ti-6Al-4V builds

Table 2: Re-raking in Ti-6Al-4V before hoppers empty out

Build serial number	Number of layers printed	Layer number at which first hopper showed evidence of emptying	Number of re-raked layers prior to hopper emptying	Percentage of layers before hopper emptying with re-raking
1	3858	1500	45	3 %
2	1854	1500	174	11.6 %
3	4500	4000	516	12.9 %
4	3500	2000	298	14.9 %
5	2500	1500	225	15.0 %

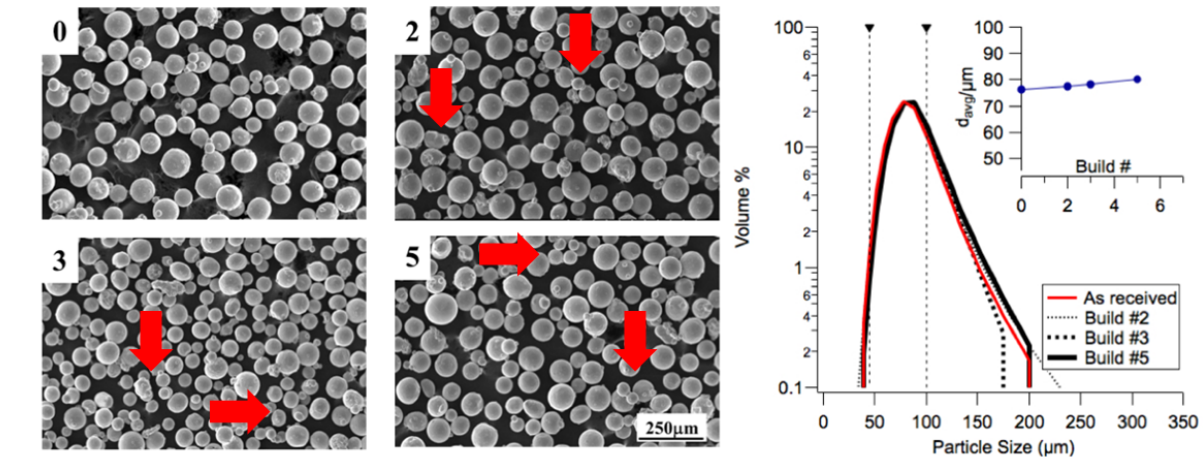

Figure 14: SEM images showing Ti-6Al-4V particle shapes after each recycling cycle and (right) particle size distribution of Ti-6Al-4V powder after different number of powder recycling cycles (reproduced from [8] with permission)

Comparing the effect of recycling on Ti-6Al-4V powder and Inconel 718 powder, we note that Inconel 718 powder exhibits increased rake passes with increase in powder recycling after build 3 whereas Ti-6Al-4V powder exhibits nearly constant re-raking from the second build itself. Following the data analysis framework proposed in this paper, we reach conclusions about the *in situ* powder spreadability of Inconel 718 and Ti-6Al-4V powders based on their sintering.

The sintering kinetics of powders depend on the particle size distribution, surface, boundary and volume diffusivities [25,26]. In this paper, we focus on the diffusivity effects alone to rationalize the observed behavior. The processing temperature of Ti-6Al-4V builds range from 500 to 700°C. At this temperature, both BCC (β-phase) and HCP (α-phase) structures are expected in this alloy. Because the diffusivity of elements in β-phase is higher than that of the α-phase, we can assume that the sintering kinetics may be accelerated by the presence of β-phase. The self-diffusivity of titanium in β-phase is on the order of 10^{-15} m^2/s at 700°C [27]. From the build log files, we found that the median build time for Ti-6Al-4V builds is 38 seconds per layer and while for Inconel 718 builds, it is 84 seconds per layer. This can be considered the median residence time for powder in the powder mound, waiting to be spread on the build platform. During this wait time, the powder could be sintered due to contact with the heated build plate. Using the residence time, we can calculate the random walk diffusion distance ($2\ X\ \sqrt{Diff\ X\ Time}$) to be 39 µm for titanium. In contrast, the processing temperature of Inconel 718 build ranges from 850°C to 1000°C. At these temperatures, the stable phase is FCC structure and the self-diffusivity of nickel in FCC-phase is on the order of 10^{-16} m^2/s at 850°C [28]. By using the measured residence time for each layer in Inconel 718 (84 seconds), the diffusion distance is 18 µm. It is indeed clear from the calculations that the sintering kinetics of Ti-6Al-4V will be at least twice as fast as Inconel 718 for every layer.

The calculated sintering kinetics and observed rake behavior may explain *in situ* powder spreadability: In the first few layers of a Ti-6Al-4V build, mostly fresh, un-sintered powder is spread across the powder bed and therefore there is minimal re-raking. We hypothesize that over time the powder deposited from the hopper -as a mound on either end of the powder bed- sinters due to heat from the powder bed. After sufficient time has passed, partially sintered powder from either end of the powder bed is being spread on the bed. This leads to short rake sensor pulses due to poor spreadability of powder with sintered agglomerates. Since this behavior is not dependent on powder recycling but on the sintering kinetics of Ti-6Al-4V itself, we expect to observe re-raking in the early builds itself; re-raking is seen from build 2 (i.e. after 1 reuse cycle). However, fast sintering would also lead to large particles that get sieved out at the end of each build and thus sintered agglomerates would not persist across builds. This conclusion is supported by SEM images in Figure 14. In Inconel 718, sintering in powder mound is expected to be sluggish in the time between replenishment of the powder mounds, compared to Ti-6Al-4V. But, slow sintering of all the Inconel 718 powder is expected to sustain across reuse cycles since slow sintering leads to particles that are small enough to pass through the sieve. This explains why powder sintering is seen in later builds of Inconel 718 (after Build 3) and increases visibly with recycling beyond three cycles (see red arrows in Figure 12).

In the series of Ti-6Al-4V builds, the first build exhibits significantly lower re-raking compared to other builds. We believe that this is because of the dryness of fresh powders and lack of oxygen pickup in fresh powder. With just one cycle of reuse, sufficient moisture and oxygen pickup may have occurred during the build process and during powder recovery and that may have led to significant increase in sintering in Build 2 and in further recycled powders.

Understanding *in situ* powder behavior during powder recycling of two commonly used alloys Ti-6Al-4V and Inconel 718 is an important result of log file data analysis as done in this paper. In terms of additional build time due to re-raking: each re-rake pass takes ~3-4 seconds of time. For a 21 hour build (Inconel 718- build 6) that had maximum re-raking (276 re-rake passes), the additional time due to re-raking is ~ 10-18 minutes which is less than 2% of the total build time. So, time taken by itself may not indicate build abnormalities. Using log file data analysis demonstrates a non-invasive method to understand *in situ* powder spreadability which can lead to build quality issues.

6. Conclusions

In this paper, the effect of powder recycling on *in situ* powder spreadability in the E-PBF process was studied. This study demonstrated that it is possible to extract value from log file data by using it to infer powder particle behavior during a build.

Based on data analysis of parts built using recycled powder, we found that Inconel 718 powder tends to agglomerate over multiple cycles of recycling. This is in contrast to Ti-6Al-4V powder where the powder seems to sinter quickly, irrespective of recycling. This indicates that additive manufacturing of Ti-6Al-4V powders needs different process conditions to account for its quick sintering behavior compared to Inconel 718. This study can also be extended by using the data analysis methodology described here to understand *in situ* powder spreadability in E-PBF process for other powders. This makes log file analysis a valuable tool for analysis of Arcam EBM ® builds.

Further validation of results about *in situ* powder behavior and spreadability in this paper could be done using Discrete Element Method (DEM) simulations of powder behavior [29–33], though this is beyond

the scope of the current work. Integrating sintering kinetics with a DEM based approach could enable better appreciation for the physics involved in AM and translate into better parameter choice for AM builds.

7. Acknowledgments

The authors would like to acknowledge the Lloyd's Register Foundation and the International Joint Research Center for the Safety of Nuclear Energy for funding of this research. Lloyd's Register Foundation helps to protect life and property by supporting engineering-related education, public engagement, and the application of research. Experimental work in this paper was sponsored by the U.S. Department of Energy, Office of Energy Efficiency and Renewable Energy, Advanced Manufacturing Office, under contract DE-AC05-00OR22725 with UT-Battelle, LLC. Experimental work at the Oak Ridge National Laboratory's High Temperature Materials Laboratory was sponsored by the U.S. Department of Energy, Office of Energy Efficiency and Renewable Energy, Vehicle Technologies Program.

Appendix:

The log file data used for analysis in this paper is available at: https://doi.org/10.7290/n8lx7b8

References

[1] Y. Zhong, L.-E. Rännar, L. Liu, A. Koptyug, S. Wikman, J. Olsen, D. Cui, Z. Shen, Additive manufacturing of 316L stainless steel by electron beam melting for nuclear fusion applications, Journal of Nuclear Materials. 486 (2017) 234–245. https://doi.org/10.1016/j.jnucmat.2016.12.042.

[2] V. Petrovic, R. Niñerola, Powder recyclability in electron beam melting for aeronautical use, Aircraft Engineering and Aerospace Technology. 87 (2015) 147–155. https://doi.org/10.1108/AEAT-11-2013-0212.

[3] L.E. Murr, E.V. Esquivel, S.A. Quinones, S.M. Gaytan, M.I. Lopez, E.Y. Martinez, F. Medina, D.H. Hernandez, E. Martinez, J.L. Martinez, S.W. Stafford, D.K. Brown, T. Hoppe, W. Meyers, U. Lindhe, R.B. Wicker, Microstructures and mechanical properties of electron beam-rapid manufactured Ti–6Al–4V biomedical prototypes compared to wrought Ti–6Al–4V, Materials Characterization. 60 (2009) 96–105. https://doi.org/10.1016/j.matchar.2008.07.006.

[4] H.P. Tang, M. Qian, N. Liu, X.Z. Zhang, G.Y. Yang, J. Wang, Effect of Powder Reuse Times on Additive Manufacturing of Ti-6Al-4V by Selective Electron Beam Melting, JOM. 67 (2015) 555–563. https://doi.org/10.1007/s11837-015-1300-4.

[5] A. Strondl, O. Lyckfeldt, H. Brodin, U. Ackelid, Characterization and Control of Powder Properties for Additive Manufacturing, JOM. 67 (2015) 549–554. https://doi.org/10.1007/s11837-015-1304-0.

[6] A. Mohammadhosseini, D. Fraser, S.H. Masood, M. Jahedi, A Study of Morphology of Titanium Powder Used in Electron Beam Melting, Applied Mechanics and Materials. 541–542 (2014) 160–163. https://doi.org/10.4028/www.scientific.net/AMM.541-542.160.

[7] Y. Sun, M. Aindow, R.J. Hebert, The effect of recycling on the oxygen distribution in Ti-6Al-4V powder for additive manufacturing, Materials at High Temperatures. 35 (2018) 217–224. https://doi.org/10.1080/09603409.2017.1389133.

[8] P. Nandwana, W.H. Peter, R.R. Dehoff, L.E. Lowe, M.M. Kirka, F. Medina, S.S. Babu, Recyclability Study on Inconel 718 and Ti-6Al-4V Powders for Use in Electron Beam Melting, Metall and Materi Trans B. 47 (2016) 754–762. https://doi.org/10.1007/s11663-015-0477-9.

[9] R.I. Jaffee, I.E. Campbell, The effect of oxygen, nitrogen, and hydrogen on iodide refined titanium, JOM. 1 (1949) 646–654. https://doi.org/10.1007/BF03398910.

[10] M. Yan, W. Xu, M.S. Dargusch, H.P. Tang, M. Brandt, M. Qian, Review of effect of oxygen on room temperature ductility of titanium and titanium alloys, Powder Metallurgy. 57 (2014) 251–257. https://doi.org/10.1179/1743290114Y.0000000108.

[11] G. Welsch, W. Bunk, Deformation Modes of the alpha-Phase of Ti-6AI-4V as a Function of Oxygen Concentration and Aging Temperature, MTA. 13 (1982) 889–899. https://doi.org/10.1007/BF02642403.

[12] Z. Liu, G. Welsch, Effects of oxygen and heat treatment on the mechanical properties of alpha and beta titanium alloys, MTA. 19 (1988) 527–542. https://doi.org/10.1007/BF02649267.

[13] V.V. Popov, A. Katz-Demyanetz, A. Garkun, M. Bamberger, The effect of powder recycling on the mechanical properties and microstructure of electron beam melted Ti-6Al-4 V specimens, Additive Manufacturing. 22 (2018) 834–843. https://doi.org/10.1016/j.addma.2018.06.003.

[14] L.C. Ardila, F. Garciandia, J.B. González-Díaz, P. Álvarez, A. Echeverria, M.M. Petite, R. Deffley, J. Ochoa, Effect of IN718 Recycled Powder Reuse on Properties of Parts Manufactured by Means of Selective Laser Melting, Physics Procedia. 56 (2014) 99–107. https://doi.org/10.1016/j.phpro.2014.08.152.

[15] Q.B. Nguyen, M.L.S. Nai, Z. Zhu, C.-N. Sun, J. Wei, W. Zhou, Characteristics of Inconel Powders for Powder-Bed Additive Manufacturing, Engineering. 3 (2017) 695–700. https://doi.org/10.1016/J.ENG.2017.05.012.
[16] L. Cordova, M. Campos, T. Tinga, Revealing the Effects of Powder Reuse for Selective Laser Melting by Powder Characterization, JOM. 71 (2019) 1062–1072. https://doi.org/10.1007/s11837-018-3305-2.
[17] J.A. Slotwinski, E.J. Garboczi, P.E. Stutzman, C.F. Ferraris, S.S. Watson, M.A. Peltz, Characterization of Metal Powders Used for Additive Manufacturing, Journal of Research of the National Institute of Standards and Technology. 119 (2014) 460. https://doi.org/10.6028/jres.119.018.
[18] W. Sames, Additive Manufacturing of Inconel 718 using Electron Beam Melting: Processing, Post-Processing, & Mechanical Properties, Thesis, 2015. https://oaktrust.library.tamu.edu/handle/1969.1/155230 (accessed July 24, 2019).
[19] M. Grasso, F. Gallina, B.M. Colosimo, Data fusion methods for statistical process monitoring and quality characterization in metal additive manufacturing, Procedia CIRP. 75 (2018) 103–107. https://doi.org/10.1016/j.procir.2018.04.045.
[20] Z.C. Cordero, H.M. Meyer, P. Nandwana, R.R. Dehoff, Powder bed charging during electron-beam additive manufacturing, Acta Materialia. 124 (2017) 437–445. https://doi.org/10.1016/j.actamat.2016.11.012.
[21] Arcam, Arcam A2 user manual, Arcam EBM User's Manual. (2011).
[22] Z. Snow, R. Martukanitz, S. Joshi, On the development of powder spreadability metrics and feedstock requirements for powder bed fusion additive manufacturing, Additive Manufacturing. 28 (2019) 78–86. https://doi.org/10.1016/j.addma.2019.04.017.
[23] M. Renderos, F. Girot, A. Lamikiz, A. Torregaray, N. Saintier, Ni Based Powder Reconditioning and Reuse for LMD Process | Elsevier Enhanced Reader, Physics Procedia. 83 (2016) 769–777. https://doi.org/10.1016/j.phpro.2016.08.079.
[24] M. Renderos, A. Torregaray, M.E. Gutierrez-Orrantia, A. Lamikiz, N. Saintier, F. Girot, Microstructure characterization of recycled IN718 powder and resulting laser clad material, Materials Characterization. 134 (2017) 103–113. https://doi.org/10.1016/j.matchar.2017.09.029.
[25] M.F. Ashby, A first report on sintering diagrams - ScienceDirect, Acta Metallurgica. 22 (1974) 275–289. https://doi.org/10.1016/0001-6160(74)90167-9.
[26] F.B. Swinkels, M.F. Ashby, A second report on sintering diagrams, Acta Metallurgica. 29 (1981) 259–281. https://doi.org/10.1016/0001-6160(81)90154-1.
[27] Diffusion in titanium and titanium alloys, in: Technical Documentary Report No. ASD-TDR-62-561, 1962: p. 67. http://www.dtic.mil/dtic/tr/fulltext/u2/290336.pdf.
[28] E.W. De Reca, C. Pampillo, Self-diffusion of Ni in Ni-Fe alloys, Acta Metallurgica. 15 (1967) 1263–1268. https://doi.org/10.1016/0001-6160(67)90001-6.
[29] J.C. Steuben, A.P. Iliopoulos, J.G. Michopoulos, Discrete element modeling of particle-based additive manufacturing processes, Computer Methods in Applied Mechanics and Engineering. 305 (2016) 537–561. https://doi.org/10.1016/j.cma.2016.02.023.
[30] W.-H. Lee, Y. Zhang, J. Zhang, Discrete element modeling of powder flow and laser heating in direct metal laser sintering process, Powder Technology. 315 (2017) 300–308. https://doi.org/10.1016/j.powtec.2017.04.002.
[31] S. Haeri, Y. Wang, O. Ghita, J. Sun, Discrete element simulation and experimental study of powder spreading process in additive manufacturing, Powder Technology. 306 (2017) 45–54. https://doi.org/10.1016/j.powtec.2016.11.002.

[32] E.J.R. Parteli, T. Pöschel, Particle-based simulation of powder application in additive manufacturing, Powder Technology. 288 (2016) 96–102. https://doi.org/10.1016/j.powtec.2015.10.035.
[33] Y.S. Lee, W. Zhang, Mesoscopic Simulation of Heat Transfer and Fluid Flow in Laser Powder Bed Additive Manufacturing, in: International Solid Freeform Fabrication Symposium, 2015: pp. 1154–1165.